

An Inverse Look at the Center of M15

Dalia Chakrabarty

School of Physics & Astronomy

University of Nottingham

Nottingham NG7 2RD

U.K.

email: dalia.chakrabarty@nottingham.ac.uk

ABSTRACT

The observed radial velocities and transverse velocities of individual stars in the globular cluster M15 are implemented as inputs to a fully non-parametric code (CHASSIS) in order to estimate the equilibrium stellar distribution function and the three-dimensional mass density profile, from which are estimated the mass-to-light ratio, enclosed mass and velocity dispersion profiles. In particular, the paper explores the possibility of the existence of a central black hole in M15 via several runs that utilize the radial velocity data set which offers kinematic measurements closer to the centre of the cluster than the proper motion data. These runs are distinguished from each other in the choice of the initial seed for the cluster characteristics; however, the profiles identified by the algorithm at the end of each run concur with each other, within error bars, thus confirming the robustness of CHASSIS. The recovered density profiles are noted to exhibit unequivocal flattening, inner to about 0.0525pc. Also, the enclosed mass profile is very close to being a power-law function of radius inside 0.1pc and is not horizontal. Simplistically speaking, these trends negate the possibility of the central mass to be concentrated in a black hole, the lower bound on the radius of the sphere of influence of which would be $\gtrsim 0.041$ pc, had it existed. However, proper analysis suggests that the mass enclosed within the inner 0.01pc could be in the form of a black hole of mass $\sim 10^3 M_{\odot}$, under two different scenarios, which are discussed. The line-of-sight velocity dispersion is visually found to be very similar to the observed dispersion profile. The enclosed mass and velocity dispersion profiles calculated from runs done with the proper motion data are found to be consistent with the profiles obtained with the radial velocity data.

Subject headings: galaxy: kinematics and dynamics—galaxy: globular clusters: individual (M15)

1. Introduction

Intermediate Mass Black Holes (IMBH) can serve as vincula to bridge the discontinuity that is otherwise apparent between the extremities of the black hole mass distribution. Lately, observational data, indicating the possible existence of IMBHs, has been accruing; some of the recent analyses are due to Portegies Zwart et al. (2004), Roberts et al. (2004), Terashima & Wilson (2004) and Cropper et al. (2004), among others. A comprehensive review of the subject of IMBH, including similar pieces of observational evidence, is presented in Miller & Colbert (2004). The case for these intermediate mass black holes has also been buttressed by the predictions of a black hole of mass of the order of $10^3 M_{\odot}$ in the center of the globular cluster M15 by Gebhardt et al. (1997) and Gerssen et al. (2002). However, the analysis by Baumgardt et al. (2003a) implies a model for the central structure of M15 that does not necessarily require a central black hole.

The paradigm of globular cluster evolution that we are aware of, from works by Spitzer (1987) and Meylan & Heggie (1997), is indeed challenged if an IMBH is needed to model a globular cluster such as M15. According to conventional understanding, in a globular cluster with few primordial binaries, core collapse is stalled by the formation of binaries via three-body processes. By the time core collapse is halted, the central density in the cluster is quite high, but this happens on time scales of the order of a few gigayears, (many times the half-mass relaxation time). In other words, such clusters spend a long time with cores in their centers. Runaway growth of a massive object can occur via collisional processes, and result in an IMBH, if circumstances are right. Portegies Zwart & McMillan (2002) suggest that runaway growth is possible in clusters with initial half mass relaxation times less than 25Myr; they also indicate that the same for M15 is probably higher than this figure. Moreover, on the basis of their modelling, Portegies Zwart & McMillan (2002) also suggest that star clusters older than about 5Myrs and current half-mass relaxation times $\lesssim 100$ Myrs are expected to contain an IMBH. The current half mass relaxation time of M15 is about 2.24Gyrs (Harris 1996), which is nearly 25 times higher than this limiting value of 100Myrs. Thus, it is unlikely that an IMBH has formed in the center of M15 by a runaway process. An alternative mechanism that could potentially form IMBHs in the centers of dense stellar clusters was suggested by Miller & Hamilton (2002). In this picture, an initial seed is contemplated to undergo a gradual collisional growth to transform into a massive object.

Thus, if claims of an IMBH in M15 are true, then we can ratiocinate that a fresh approach needs to be invoked in order to understand globular cluster evolution. In light of such profound implications of these predictions, it is important to make an independent evaluation of the central structure of M15. This is attempted in this paper. The algorithm

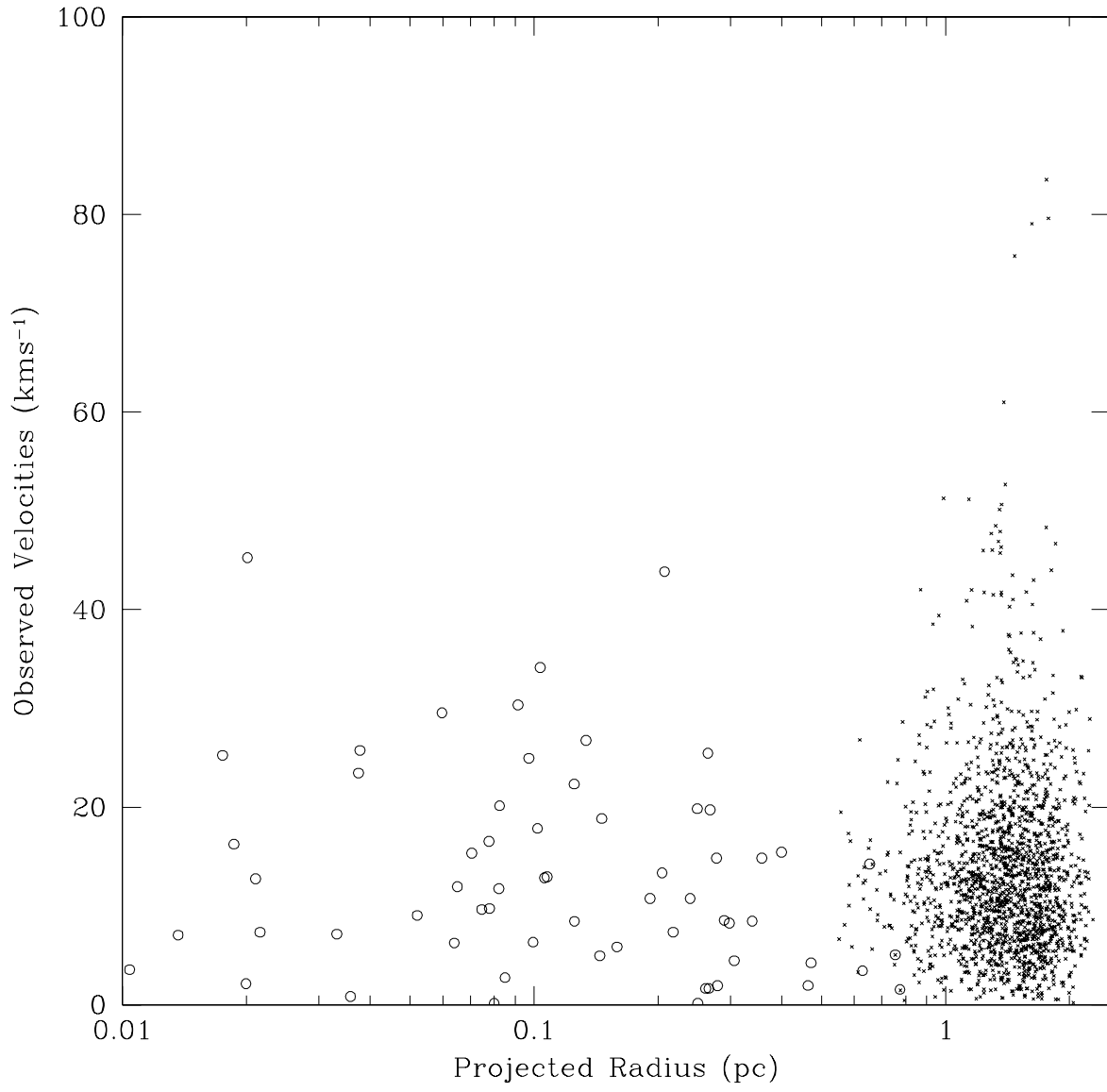
used in this exercise is a fully non-parametric code (CHASSIS) that was used to constrain the mass of the central black hole in our Galaxy (Chakrabarty & Saha 2001) and was calibrated against N-body realizations of the Hyades (Portegies Zwart et al. 2001) and Arches (Portegies Zwart et al. 2002) clusters (Chakrabarty & Portegies Zwart 2004). The input data for this algorithm is taken from the observed radial velocities of 64 stars in M15 (Gerssen et al. 2002) and the observed proper motions of 1764 stars in this globular cluster (McNamara, Harrison & Anderson 2003).

This introductory section is followed by a brief mention of the salient points of the data sets that have been used as inputs to the algorithm. In Section 3, the basic scheme of CHASSIS is briefly discussed. A description of the procedure followed in this paper, to calculate the mass-to-light ratio, has been discussed in Section 4. The results obtained by the algorithm are presented in Section 5. This is followed by Section 6. Finally, the paper is rounded up by a conclusive section.

2. Data

Gerssen et al. (2002) present radial velocities of 64 stars obtained by the Space Telescope Imaging Spectrograph (STIS) on HST. This sample of stars is characterized by very high spatial resolution; the smallest radius at which kinematic information is available in the sample (r_{\min}) is only about 0.01pc. This data set is shown in Figure 1. Gerssen et al. (2002) surmised that two of the stars in this sample were RR Lyrae variables which can have velocity variations characterized by amplitudes of the order of 50kms^{-1} . Therefore, this pair of stars was ignored when the input data was ported off to the algorithm.

McNamara, Harrison & Anderson (2003) present the internal proper motions of 1764 stars in M15. This data was taken with the *HST* Wide Field Planetary Camera 2 (WFPC2). The observed proper motions are transformed into transverse velocities, using the distance D to M15 of 10kpc, which was the value adopted by the observers and is compatible with the value (of 9.98 ± 0.47) according to McNamara, Harrison & Baumgardt (2004). The set of transverse velocities is plotted against the observed apparent positions in Figure 1. This data set is taken over a much larger radial range (from 0.55pc to 2.28pc, approximately) though r_{\min} is nearly 55 times larger in this data set than in the radial velocity sample. The transverse velocities (v_{μ}) are calculated as the quadrature of the proper motions μ_x and μ_y , scaled to units of kms^{-1} . Figure 1 represents the observed kinematic data in a plot against apparent position. The open circles symbolize the STIS data while the transverse velocities are shown by dots. The absolute of the difference between a radial velocity value and the mean of the radial velocities is depicted while the transverse velocities are scaled down by a



factor of $\sqrt{2}$ since two components of the velocity vector define them.

3. Algorithm

As mentioned in Section 1, the algorithm CHASSIS (CHAracterizing Stellar Systems with a new Inverse Scheme) has been used before (Chakrabarty & Saha 2001; Chakrabarty & Portegies Zwart 2004). It is a fully non-parametric code that attempts to simultaneously identify the pair of phase space distribution function (DF) and the potential, (rather the density from which the potential is subsequently calculated) that best describe the stellar system at hand. This it does via a maximum likelihood approach. In its current version, CHASSIS recovers the system characteristics under the assumptions of sphericity and isotropy in velocity space. Actually, core collapse clusters are prone to becoming radially anisotropic in the central regions (Baumgardt et al. 2003c), but this anisotropy is perceived to be small in the case of M15, at least in the radial ranges that are probed in this work. Isotropy is less bad an approximation for the runs that are performed with the radial velocity data than the proper motions, since the latter data set extends to higher radii. The maxima of the likelihood function is identified by the Metropolis algorithm.

The algorithm starts with an arbitrary pair of functions that serve as guesses for the DF and the stellar density. Potential is calculated from this density, using Poisson equation, under the assumption of sphericity. At each step, the DF is projected into the space of the observables at the current form of the potential. This produces the projected distribution function, which is rendered a function of the apparent position and the observed velocity component(s). The product of all such projected distribution functions, each corresponding to a data point in the observed data set, is the likelihood function. When the likelihood is maximum, the current choice of DF and density are said to be the functions that describe the observed data set the best.

The advantage of utilizing the Metropolis algorithm over other optimization techniques, (such as simulated annealing), is that Metropolis directly recovers the errors on the DF and density from the code; it offers a set of models as possible answers. These models are distributed according to their likelihoods. The models lying within the 16th and the 84th centiles are used to estimate the errors of the analysis. The error bars on the recovered DF and density are these 68% errors. All the other quantities of interest (such as enclosed mass and velocity dispersion profiles) which are calculated from the density and the DF, are presented with superimposed error bars that correspond to these errors in the density and DF. It may be noted that these errors stem from the uncertainties in identifying the global maxima in the likelihood function and are essentially different from the observational errors.

The errors in the velocity measurements are incorporated into the analysis by convolving the projected distribution function with the distribution of the observational errors, (assumed Gaussian). For greater details about CHASSIS see Chakrabarty & Saha (2001).

4. Mass-to-Light Ratio

One interesting quantity to estimate from the density distribution recovered by CHASSIS and the photometry of M15, is the mass-to-light ratio. The three dimensional mass density identified by CHASSIS can be projected along the line-of-sight to give the surface mass density profile of M15. Now, Sosin & King (1997) provide the surface brightness of M15 from deep *HST* imaging of M15. The data in Sosin & King (1997) is in the form of star counts per square arcsecond while we have the mass per arcsecond square from the recovered surface mass density profile. Therefore, what we need to calculate the mass to light ratio (Υ) at any radius, is information on the photometry of M15. This has been taken from the catalogues presented by Trager, King & Djorgovski (1995), who provide the surface brightness profile of M15 in the *V*-band.

The quantity that we seek is formally defined as:

$$\Upsilon_X(r) = M(r)/N_X(r), \quad (1)$$

where $\Upsilon_X(r)$ is the mass-to-light ratio at radius r , in the waveband X . $M(r)$ is the mass of the system in solar masses, at radius r and $N_X(r)$ is defined as the number of Suns, which when placed at the distance of M15 (10kpc), would produce the observed flux at waveband X , at radius r . Then in the *V*-band, $N_V(r)$ will be given in terms of the intensity ($\mu_V(r)$) at radius r and apparent magnitude ($m_{\odot V}$) of the Sun at the distance of 10kpc to M15, according to the following prescription:

$$N_V(r) = 10^{\frac{m_{\odot V} - \mu_V(r)}{2.5}} \quad (2)$$

Now, $m_{\odot V} = M_{\odot V} + \log(10 \times 10^3/10) = 19.83$, where $M_{\odot V}$ is the absolute magnitude of the Sun in the *V*-band (=4.830). The observed surface brightness in the central region is possibly erroneous owing to seeing difficulties. This is averted by normalizing the surface brightness profile by the value at a radial location where seeing is least likely to be problem, (namely, the outermost radius in the star counts data set) using the star counts data reported by Sosin & King (1997).

The errors in the presented mass-to-light profiles correspond to the 1- σ errors in the estimation of the surface density, compounded by the observational errors in the star count profile, obtained from the data in Sosin & King (1997).

5. Results

A typical feature of all iterative schemes is the requirement of an initial guess corresponding to the answer that the scheme seeks. If the algorithm is robust in its design, then the answer will not depend on the choice of this guess; it is crucial to establish such robustness on every occasion. CHASSIS has been shown to be robust to the choice of the initial guesses for the distribution function and density profile, in its past applications. The independence of the answers to such choice is discussed below, in reference to runs that are carried out with the input data set comprised of radial velocity measurements. Since this data set extends more towards the central parts of M15 and is better resolved than the proper motion data, it is more suitable for such analysis.

Now, the form of the density profile that was used as this initial guess is chosen such that it is characterized by four parameters: a scale $\tilde{\rho}_0$, a core radius r_c and two steepness parameters, α and β :

$$\tilde{\rho}(r) = \frac{\tilde{\rho}_0}{\left[1 + \left(\frac{r}{r_c}\right)^\alpha\right]^{2\beta}} \quad (3)$$

Assigning values of 2 and 3/4 to α and β respectively, renders the line-of-sight projection of this guess for the initial form of the density distribution analytical.

At the beginning of the algorithm, the distribution function is conjectured to be of a form that involves a single free parameter only:

$$f(\epsilon) = \exp(\epsilon^\gamma) \quad (4)$$

where ϵ is the effective energy. The distribution function is normalized such that its value at the highest effective energy is unity.

Runs have been performed with assorted values of each of the parameters present in the functional forms of the initial guesses for the density and the distribution function. The results from these various runs have been compared for consistency, to bring forth the degree of independence of the results from the choice of the initial guess for the density and distribution function. For easy interpretation, when one parameter is changed over a wide range of values, the others are held constant.

5.1. Effect of changing the initial guess for density

Experiments indicated that the overall scale or amplitude assigned to the guess for the density distribution does not have any impact on the results. Even when the amplitude of

the initial (guessed) density profile is varied over 12 orders of magnitude, Metropolis moves “very quickly” to a unique density profile (i.e. the answer) - “very quickly” implies within 10% of the number of steps that are required for convergence.

Therefore, the effective number of free parameters in the guess for the density is three. Three sets of runs were performed to check the effects of varying these three parameters. Each such set consists of two runs; the two runs (RUN1 and RUN2) in the first set were marked by β set to 2 and 3, while r_c , α and γ were held constant at 0.001pc, 3.8, 1, respectively. Next, α was set to 1.8 (RUN3) for one run and later to 5.8 (RUN4); during both these runs, β , r_c and γ were set to 1, 0.001pc and 1, respectively. The third set of runs (RUN5 and RUN6) were carried out with two varying values of the core radius - r_c was assigned the values of 0.1pc and 0.00001pc while maintaining β , α and γ at 3.8, 1, 1, respectively. The setup of each of these runs is tabulated in Table 1.

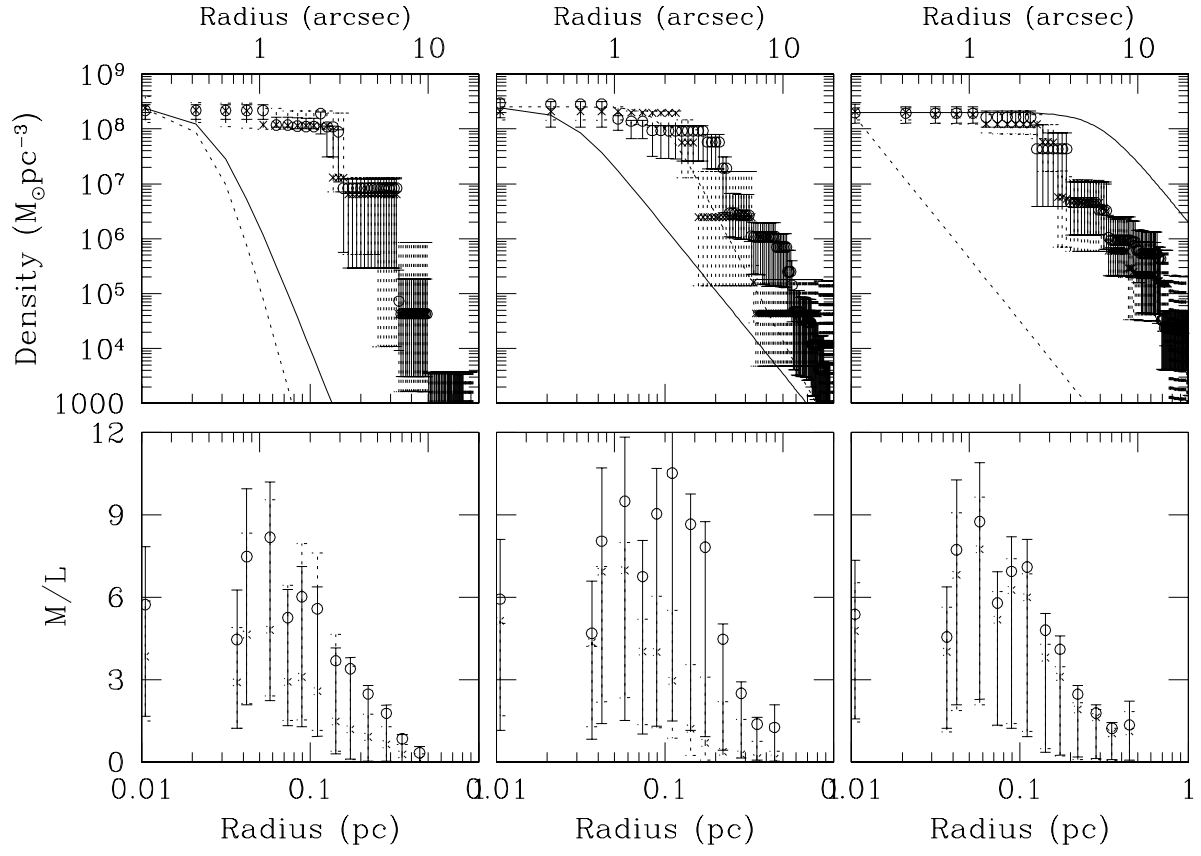
The forms of the initial guess in each set of runs and the corresponding recovered density distributions are shown in the top panels of Figure 2. Density profiles identified by the algorithm from runs done with two varying values of the same parameter are overplotted to aid a visual comparison of the degree of overlap between the results and the extent by which an achieved profile is distant from the initial guess for the same.

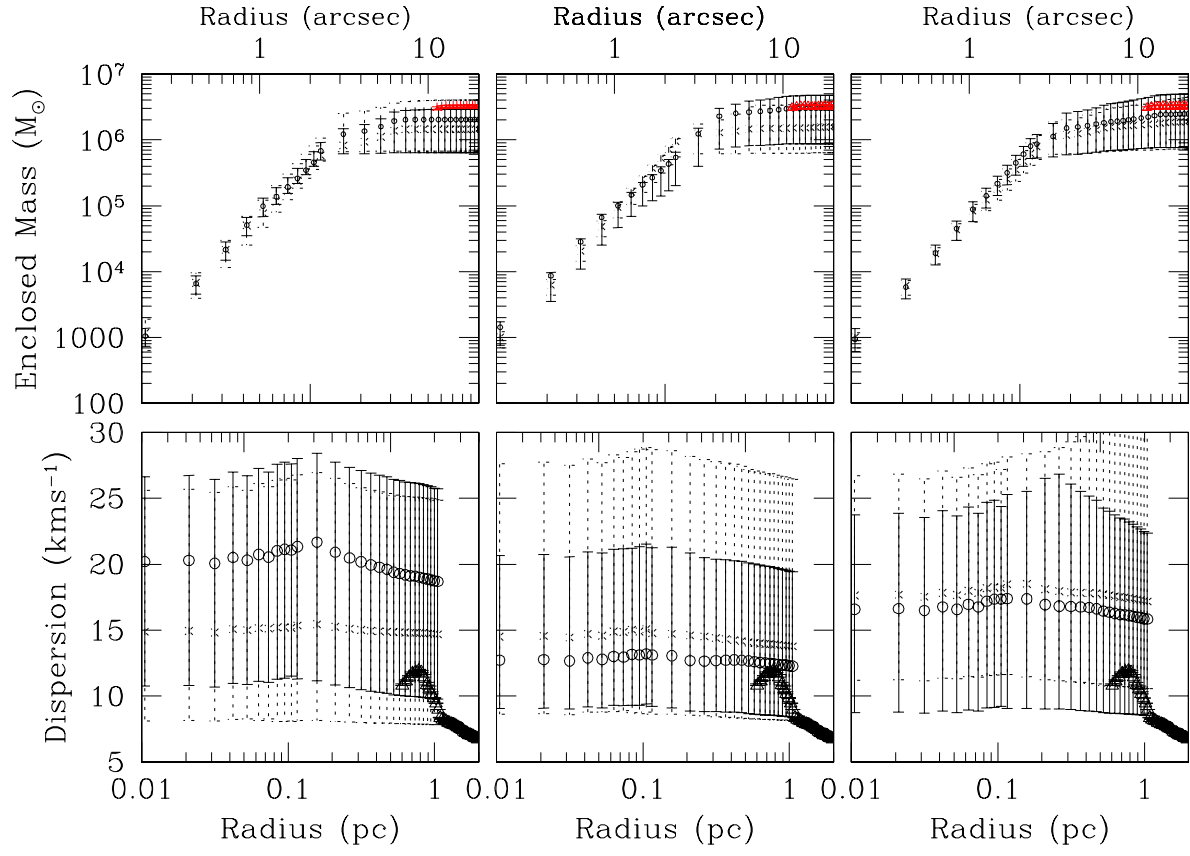
As mentioned before, these density profiles are extracted with the radial velocities that are used as the input to the code. Also, the recovered profiles are the total (luminous and dark) three dimensional mass density profile of M15. In each of these runs, the radial resolution is limited from the bottom by an r_{\min} of 0.0104pc from the observations presented by Gerssen et al. (2002). We choose our radial bins to be 0.0105pc wide, just slightly higher than this r_{\min} .

The lower panels in Figure 2 display plots of the mass to light ratio against radius, corresponding to each set of runs that were performed with the different initial density configurations. The calculation of the mass-to-light ratio has been discussed before in Section 4.

Figure 3 shows the enclosed mass and velocity dispersion profiles obtained from the density distributions and distribution functions that are recovered by CHASSIS from the different runs. The mass and dispersion profiles obtained from runs using the proper motion data are superimposed on these plots. The proper motion measurements are characterized by an r_{\min} of about 0.55pc. Thus, the proper motion run was chosen to have a radial resolution of 0.035pc, with the first radial bin extending from 0.5325pc to 0.5675pc.

An important point to notice is that irrespective of the details of the run, the recovered density profile is always found to be marked by a core that extends to about 0.0525pc. Likewise, the enclosed mass profile is found to be nearly linear in the central parts and is





definitely not horizontal by the first radial bin (0.0105pc). The mass-to-light ratio profile is found to rise sharply as we go inwards; this is due to the crowding of non-luminous compact objects in the central parts of the cluster. This point is taken up for further discussion in Section 6. The presented mass-to-light profiles compare favorably with the same obtained for the best fitting models in Dull et al. (2003). Lastly, the velocity dispersion profiles estimated from the different runs appear to be consistent with that reported in Gerssen et al. (2002), upon visual inspection.

The mass and dispersion profiles found from the proper motion run sit comfortably within the error bars associated with the same quantities that are calculated from the radial velocity runs.

5.2. Effect of changing the initial guess for distribution function

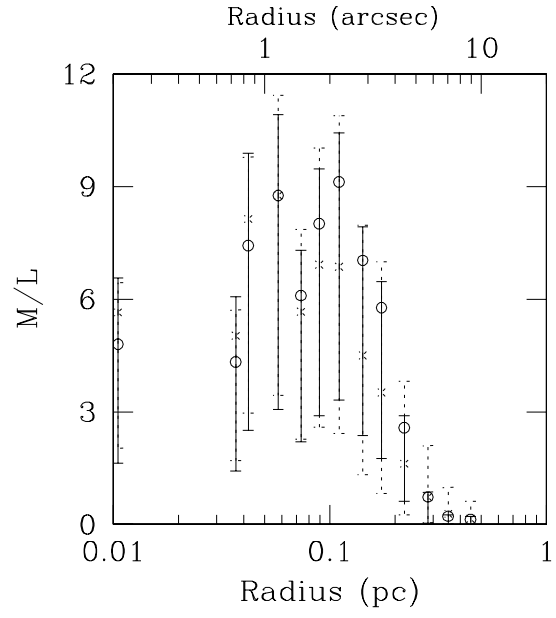
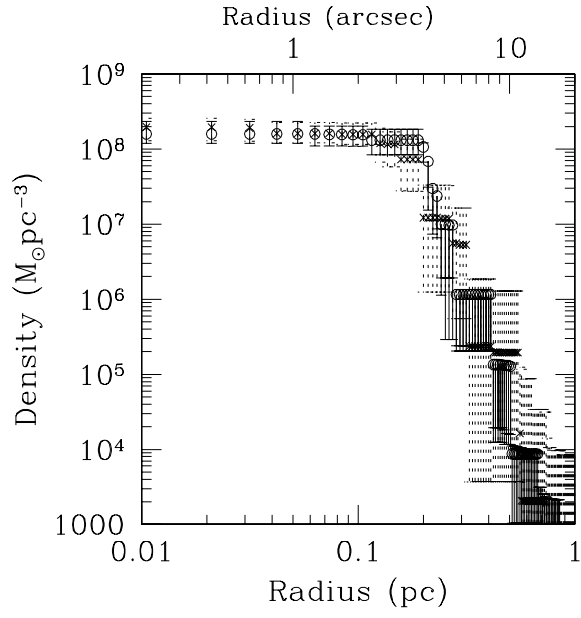
As indicated in Equation 4, the choice for the initial form of the distribution function is marked by only a single free parameter, γ . Two runs are carried out (RUN7 and RUN8), each with a distinct value of γ ($\gamma=5$ and 0.01, respectively) and the other free parameters assigned constant values, namely $\alpha = 3.8$, $r_c = 0.001pc$ and $\beta = 1$. Again, these details are repeated in a tabular form in Table 1.

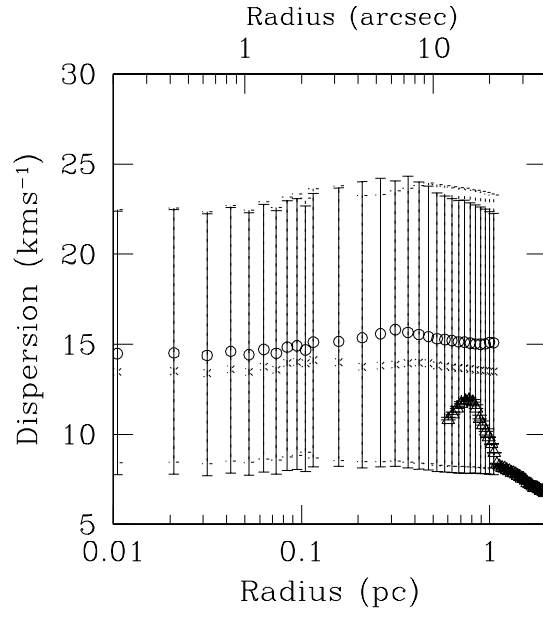
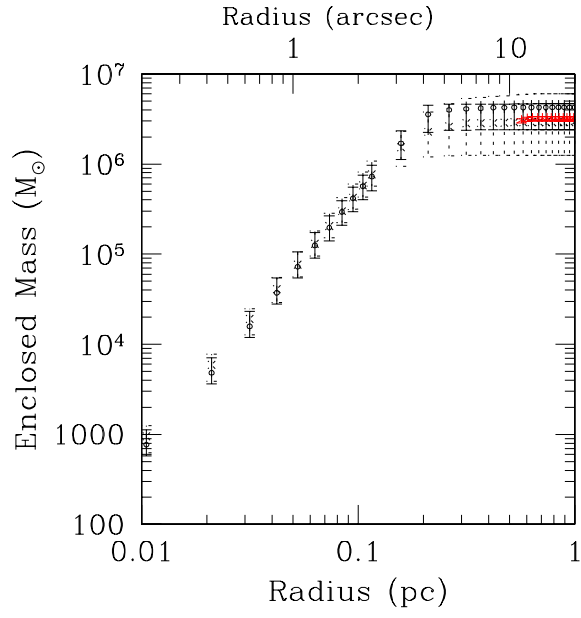
The density distributions and mass-to-light ratio profiles obtained from these runs are shown in Figure 4. Again, the core of size of about 0.0525pc is noted in the density profiles while the mass-to-light ratio appears to resemble the ones shown in Figure 2. The enclosed mass and velocity dispersion profiles, obtained from RUN7 and RUN8 are displayed in Figure 5. As with the profiles shown in Figure 3, we can see that the mass profiles do not turn horizontal till the right edge of the first radial bin used in the run.

The results obtained from the different runs (RUN1, . . . , RUN8) are tabulated in Table 2. Inspection of the results obtained from the different runs indicates strong similarities. This implies that CHASSIS is indeed robust to the selection of the initial guesses for the quantities that it hopes to identify. This and other implications of the results are discussed in Section 6.

6. Discussions

In this paper, the observed kinematic data of M15 (radial velocities by Gerssen et al. (2002) and proper motions by McNamara, Harrison & Anderson (2003)) have been analyzed non-parametrically by the algorithm CHASSIS. The focus of this work is the very central part of the cluster; the primary question that this paper attempts to answer is about the existence of





a central IMBH in M15. Since the radial velocity measurements are more centrally focused than the proper motion observations, they are more suitable as inputs for the exercise at hand.

Several runs were performed with distinct forms of the seeds for the quantities that are sought by CHASSIS. Irrespective of what the initial choices of the distribution function and density were, results from the runs were found to be consistent with each other, within the error bars. This establishes the robustness of CHASSIS in the context of the radial velocity runs and offers confidence in the results identified by the algorithm. The recovered density distributions are always found to exhibit a clear flattening at the center, for $r \leq 0.0525\text{pc}$ in most cases. The core sizes of the profiles recovered from the different runs are given in Table 2. Since the recovered density profile is the full three dimensional density distribution, such a flattening is compelling evidence of the fact that no black hole resides in the center of M15.

If a central black hole did indeed exist, then the density profile in the inner regions of the cluster would have steepened as $r^{-1.75}$, as the equilibrium stellar density is expected to, in a cluster around a black hole, (Bahcall, Wolf 1976; Baumgardt, Makino, Ebisuzaki 2004a). The mass profile in these parts would have turned nearly horizontal in this scenario. Neither profile is noted to behave this way, indicating that the *enclosed mass is not in a central black hole*. In fact, the enclosed mass profiles that were inferred on the basis of these recovered density distributions are noted to vary almost linearly with radius, inner to about 0.1pc.

Let us assume, for argument’s sake that all the mass that is found to be enclosed within the innermost radial bin (0.0105pc) is in the form of a black hole. This quantity, as obtained from the various runs, is enumerated in Table 2. Now, the size of the sphere of influence of a black hole (r_s) could be related to its mass M_{BH} and the velocity dispersion σ by:

$$r_s = \frac{GM_{BH}}{\sigma^2} \quad (5)$$

where G is the Universal Gravitation Constant. From the enclosed mass and dispersion data, it can be seen that the minimum that r_s can get is about 0.041pc. The trends in the density and mass profiles that bear the signatures of a black hole should have been apparent at a radius that is of the same order as this scale length, if the assumption that all the mass inner to 0.0105pc was in the form of a black hole.

Even under this assumption, the presented profiles suggest that such trends are absent at all $r \geq 0.0105\text{pc}$, i.e. by a location that is nearly 4 times smaller than the r_s of the most massive central black hole possible from our results. However, it is possible in principle to arrange the orbits in the central regions of the cluster in such a way that the effect of a central black hole is limited to radial locations much inner to this scale length r_s , as it is

defined above. Similarly, distributions of orbits can be conjured up such that the effect of the black hole is felt at locations much higher than the estimated r_s . Though it may be argued that it is too contrived to think up orbital distributions that suggest a range of influence that differs widely from the estimated r_s (in our case much smaller than the estimated value of r_s), it is important to include such a possibility before arriving at a definite conclusion about the presence of the IMBH in M15. In this case, we will not be able to ascertain the characteristic trends in the density and mass profiles, unless further data sets at higher resolutions are available.

It is also possible that only a fraction of the mass enclosed within the right edge of the innermost radial bin is in the form of a central IMBH. In that case, the sphere of influence of such an IMBH will be less than 0.041pc and it can be argued that steepening of the density profile (or flattening of the mass profile) is expected to show up inner to 0.0105pc. In this scenario, we could miss these trends from our runs. If this is true, the density distribution of the cluster will start steepening as $r^{-1.75}$ at some radius <0.0105 pc, after remaining flat between about 0.0525pc and this radius. In other words, the three dimensional density distribution of M15 will be a broken profile, with the cusp appearing inner to 0.0105pc. Such a cusp can be betrayed in the results only if the observations improve further in resolution.

If either of the two possibilities discussed in the last two paragraphs is (or both are) true, then under the current state of the observational data, we can only impose an upper limit on the mass that may be existent in the form of a central black hole. Values of this mass are presented in Table 2 for the different runs; the results indicate that if the hypothesized IMBH exists, the upper limit to its mass is $\sim 1000M_\odot$. If we agree that the radius of the sphere of influence of a black hole is defined as the location where the observed central velocity dispersion just balances the circular speed around the black hole, (as in Equation 5), then to miss the inner cusp in the density distribution, r_s of the assumed central IMBH has to be < 0.0105 pc. This would then imply that the upper bound on the mass of such an IMBH is about a quarter of the mass that we note to be enclosed within our innermost bin, i.e. about $250M_\odot$.

The velocity dispersion profiles obtained from runs that utilize the radial velocities in CHASSIS are noted to be similar to the run of the velocity dispersion reported by Gerssen et al. (2002). Moreover, the mass-to-light ratio profiles are found to be consistent with what is reported in Dull et al. (2003). Such findings offer confidence in the results obtained with CHASSIS.

Figure 3 and Figure 5 display the fact that when proper motions are used as the input measurements, the mass profile from the proper motion data joins in smoothly with that obtained from the radial velocities, within the error bars. There are approximately 30 times

more velocity measurements reported in the proper motion sample than in the STIS data set. This implies that the errors in the profiles recovered from the proper motion runs should be about 5.4 (which is $\approx \sqrt{30}$) times less than those derived from the radial velocity runs. The errors in the innermost bin in the enclosed mass profile estimated from the proper motion run are about 6% while these are about 30% from the radial velocity runs. Thus, what we note as the extent of the relative errors from the two types of runs is close to what is expected.

When the proper motions are used as the input to CHASSIS, the estimated dispersion and enclosed mass profiles are found to be consistent (within 1σ error bars) with the profiles identified with the radial velocity data as the input. The dispersion results from the proper motion data do however display the trend of lying on the lower side of the median level of the mass and dispersion values from the STIS data. This discrepancy might be an indication of the anisotropy that is known to affect the velocity distribution in M15. Also, incorrect estimation of the observational errors could suggest such a trend.

The run of the recovered mass to light ratio against radius shows a sharp increase towards the centre though it dips at the centre. This increasing trend itself should not be misinterpreted as the signature of a dark mass in the centre of the cluster. Had the central mass existed in the form of a black hole, the increasing trend in the M/L profile would have continued unabated to $r = 0$. It does not; the trend indicates the predominance of non-luminous compact remnants such as neutron stars and white dwarfs in the central parts of this core-collapse clusters. The effect of the lowering of the fraction of the less massive visible stars at the very centre is compounded by the significant reduction in the slope of the density profile as identified by CHASSIS, as one proceeds inwards. Baumgardt et al. (2003a) and Dull et al. (2003) identify a similar result.

The error bars in the recovered density distribution are not correlated to each other. However, when the enclosed mass profile is extracted from this density, the errors add up cumulatively. Consequently, the size of the error bars increases with radius. Thus, the fractional errors in the innermost bin are about 30% while at about 1pc the values are much higher. The fractional errors in the estimation of the line-of-sight dispersion profiles are expected to be higher than those corresponding to the other derived quantity, namely the mass profiles. This owes to three numerical integrals that are involved in the calculation of the density convolved, projected velocity dispersion profiles, as compared to the single integral that corresponds to the estimation of the enclosed mass profiles. Likewise, the errors in the mass-to-light ratio distributions are expected to be relatively high since the errors in the estimation of the density by the algorithm are compounded by the observational errors in the surface brightness profile.

The slope of the recovered mass profile of M15 appears to decrease significantly by about 1pc. At this radius, the lowest value of the enclosed mass recovered is about $6.35 \times 10^5 M_\odot$. Now, the half-mass radius of M15 is about 3pc, so even if the enclosed mass at the half-mass radius is still the same as that at 1pc, the mass of the cluster is at least as high as $1.27 \times 10^6 M_\odot$. This value of the predicted cluster mass of M15 appears to be in excess of what other workers have inferred. In Dull et al. (1997) the mass of M15 is cited as about $5 \times 10^5 M_\odot$ while McNamara, Harrison & Baumgardt (2004) find it to be about $4.5 \times 10^5 M_\odot$.

A fundamental reason why such a discrepancy exists might be explained in terms of the assumption of isotropy which is a basic tenet of CHASSIS. It might indeed be true that M15 is characterized by anisotropy in the central regions, as Baumgardt et al. (2003c) predicted for core collapsed clusters and Gebhardt et al. (2000) reported from ground based observations. The measurement of rotational velocities were improved upon by Gerssen et al. (2002) - they report a maximum rotational velocity of 13 km s^{-1} at $0.5''$. Figure 6 describes the situation in light of the assumption of isotropy in velocity space, even when the system is really anisotropic. This state of affairs is similar to that of erroneously assuming an ellipsoidal system to be spherical (see left panel of Figure 6). The picture indicated in left panel of this figure is the same as that described in Figure 12 in Chakrabarty & Portegies Zwart (2004). The assumption of sphericity leads to an overestimation of the enclosed mass, i.e. of the quantity given by the integral $\int \rho(r) d^3 \mathbf{r}$, where $\rho(r)$ is the density of a system (assumed spherical) at the point \mathbf{r} .

Along the same lines, it can be argued that assuming isotropy in velocity space, when the system is actually marked by anisotropy, helps to spuriously enhance the quantity $\int f(E) d^3 \mathbf{v}$, where $f(E)$ is the stellar distribution function at energy E which in turn is given in terms of the potential of the system and the velocity \mathbf{v} . But this integral is really the number density of stars. Thus, we see that whenever the assumption of isotropy is a mistake, the number density is artificially increased. Such an assumption is indeed erroneous near the end of the radial range considered for our runs done with the STIS data. Hence, we can expect that at such radii, the number density of stars that is recovered by CHASSIS is spuriously high. If the mass function of M15 was flat (which it is not, as reported by Sosin & vKing 1997), the number density and mass density would be directly linked. Thus, the simplistic assumption of isotropy at all radii is expected to lead to falsely large values of mass densities, at radii around 1pc.

Another way of looking at the same situation is in terms of the likelihood. The steepness of the distribution function obtained from the assumption of isotropy is expected to be different from that calculated under the assumption of anisotropy in velocity space. A steeper distribution function implies relatively lower values of f at most velocities. This

then leads to lower projected distribution function values and a lower likelihood, during any step. A lower value of the likelihood function implies a lower binding energy for the most stable orbit, i.e. less mass enclosed within the orbit. Then the question is, when is the distribution function steeper; is the profile of f against velocities steeper when isotropy is assumed or anisotropy? If the energy dependence of the distribution function is fixed, the anisotropic distribution function will be steeper. Therefore, the assumption of isotropy will lead to higher enclosed mass. Such an assumption appears erroneous at the outer edge of the considered radial range but not so in the central parts of the cluster. Hence, it is due to the assumption of isotropy at these outer parts of our considered radial range, that the enclosed mass will be rendered higher than if anisotropy were assumed.

Moreover, the lack of sufficient data points around the edge of the considered radial range could lead to the tail of the recovered mass profile being less constrained than at inner radii, leading to a spuriously high cluster mass estimate. There are 37 velocity data points inner to 0.2pc in the radial velocity data and 25 more data points that span a much larger radial range from 0.2pc to about 1pc. In fact, between 0.5pc and 1pc, there are only 4 velocity data reported in the STIS data.

Thus, it may be argued that the employment of the ground based data for M15 would have been a more judicious choice since there are many more velocity data points in this data set compared to the STIS observations. However, the ground based observations have much poorer resolution than the STIS sample. Therefore, given that the focus of this paper is the analysis of the *central* density structure of the cluster, particularly the investigation of the existence of the central IMBH in M15, the STIS data is the pertinent sample.

Thus, we see that the tail of our recovered density profile might be flatter than what the case is in M15, though the central structure is correctly predicted. The resulting discrepancy in the recovered cluster mass owes to the artifacts in the code, discussed above.

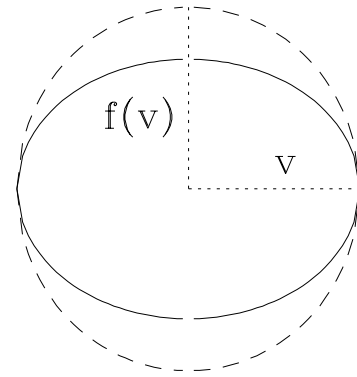
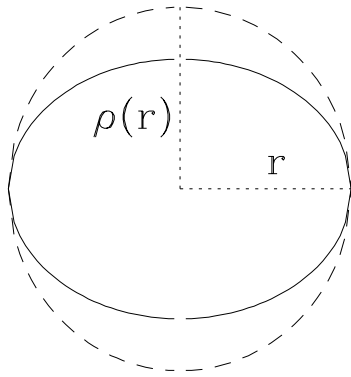
The discrepancy in the cluster mass could also be explained by carefully examining the reported mass values. In Dull et al. (1997), the reported figure is achieved by fitting the Fokker-Planck models of M15 that the authors have constructed, to the observations of surface brightness profile, velocity dispersion and the radial profile of the line-of-sight component of the accelerations of millisecond pulsars PSR 2127+11A and D. It is to be noted that the corrected version of the profile of the line-of-sight acceleration has been presented in Dull et al. (2003). This work also includes a plot of the velocity dispersion profiles corresponding to different models (with the observed data superimposed on top) over an expanded radial range. Three observations are at least required since there are three unknowns that need to be effectively constrained to define the best fit model. These are, the slope of the IMF, the total number of stars and the radial scale of the model. While the

comparison against the surface brightness profile constrained the good models quite well, the same could hardly be said about the fit to the velocity dispersion data. As is apparent from Figure 6 of the paper, or its corresponding expanded version in Dull et al. (2003), none of the models fit the dispersion data well in the range of 0.1pc to 1pc, which is to say that the good model cannot be distinguished from the unacceptable ones from this fitting exercise.

However this shortcoming still renders the mass estimate to lie very close to the prediction by McNamara, Harrison & Baumgardt (2004), who use the observed surface brightness data to determine the radial scale by which the N-body models of Baumgardt et al. (2003b) need to be adjusted. The best fitting model is then found by comparing the observed velocity proper-motions dispersion profile to the model velocity dispersions, by a χ^2 test. Gerssen et al. (2003, 2002) carry out the modeling of the M15 via the Jeans equation analysis of the observed radial velocity data (STIS data). Hence it is expected that their estimate of the total mass is a lower limit to what the true mass is, given the fact that only a projection of the three dimensional velocity dispersion profile has been used as the input to the analysis.

It is noted that the density profile suggested by CHASSIS is marked by jumps, albeit within the errors. The jumps or steps in the recovered density distribution cannot be physical of course; these are artifacts typical of any non-parametric algorithm. Traditionally, the way to smooth out profiles identified by the algorithm, has been by introducing a bias or a penalty function. However, such a smoothing function brings owes of its own kind, particularly, the answer then depends on the choice of the bias function itself. Hence, it is not the best of choices. Also, smoothing the distribution by hand is perhaps not an honest reflection of the profile that describes the data the best. Thus, the kind of profile indicated by CHASSIS is a better alternative. It is the best description of the observed data though is rendered ragged by the amplification of the shot noise, a general problem of the operation of deprojection. On projection of the density distribution, this problem disappears. The algorithm can perform better with a larger data set.

In Gerssen et al. (2003), the earlier analysis done by the same group (Gerssen et al. 2002) on the basis of varying mass-to-light ratios is amended. Consequently, the newer calculations indicate that models without a central IMBH are possible within 1σ errors. Albeit, they claim that the fit to the data is “marginally” improved by including a black hole of mass $1.7_{-1.7}^{+2.7} \times 10^3 M_{\odot}$. My analysis however differs from this inference and my results are closer to the N-body simulations of the M15 globular cluster by Baumgardt et al. (2003a) who conclude that the maximum black hole mass is $\leq 500 M_{\odot}$, in the extreme case scenario of 0% neutron star retention from the cluster at formation (the scenario invoked by Gerssen et al. (2003) to explain the presence of the central black hole). McNamara, Harrison & Anderson (2003) also claim to find little direct evidence for M15 to contain a black hole at



its center. Baumgardt, Makino, Ebisuzaki (2004a,b) report the evolution of clusters that have been assigned central black holes to start with. These are interesting simulations in which it is studied how such a cluster would look in projection and how easy it is to detect the central IMBH in such a cluster. Baumgardt, Makino, Ebisuzaki (2004b) deal with a realistic mass spectra for the considered clusters; they report that a density cusp forms around the assigned central black hole, with the slope of $r^{-1.55}$. Their paper also states that the presence of IMBHs in "galactic core collapsed clusters like M15 is ruled out". This conclusion is compatible with the findings reported in the current paper, in regard to M15.

7. Conclusions

This paper reports the characteristics of the globular cluster M15, as estimated by the algorithm CHASSIS. To achieve this, the observed radial velocities and proper motions of individual stars in M15 are implemented as inputs to the code. The recovered three dimensional mass density distribution is found to be distinguished by a core central to about 0.0525pc. The enclosed mass profile that is calculated from this density distribution is noted to have the form of a single power-law in radius, inner to about 0.1pc. These distinct features appear to be in contradiction with a hypothesis that supports a central IMBH in M15. This argument appears to be further buttressed by the following rationale.

The mass that is found to be enclosed within the innermost radial bin (the extent of which corresponds roughly to the innermost radial location at which a velocity information is reported) at 0.0105pc is of the order of $1000M_{\odot}$. If we assume that this mass was entirely in the form of a central black hole, the radius of the sphere of influence of such a black hole (r_s) is found to be at least as high as 0.041pc. Here, r_s is calculated as the radius at which the observed (or estimated) central velocity dispersion equals the circular velocity around the black hole, (see Equation 5). Since this value is nearly 4 times the innermost radius at which the expected trends in the density and mass profiles are noted to be absent, the inference is that there exists no IMBH at the M15 centre. However, such a conclusion can be challenged in the following ways; firstly the assumption that all the mass is in a black hole maybe wrong. Secondly, the extent of the influence of a central black hole is dependant on the phase space distribution and various forms of this could yield values of r_s that may differ by a factor of few from the value that Equation 5 yields.

If only a fraction of the mass that is enclosed within the first radial bin is in the form of a black hole, then the sphere of influence of such a black hole would be proportionately smaller than 0.041pc. It is possible that it is even interior to the edge of our first bin. In this case, we would not be able to spot the expected trends in our reslts, unless the resolution

of the observed kinematic data sets improved. Of course the density profile then would be broken; density will rise steeply at some radius $< 0.0105\text{pc}$, after staying flat 0.0525pc inwards, approximately. In this scenario, for us to miss the tell tale signs of the central IMBH, r_s of this black hole, as given by Equation 5, has to be $< 0.0105\text{pc}$. This implies that the mass of this IMBH will be less than about a quarter of the mass that is found enclosed within the first radial bin (presented in Table 2).

The other source of possible concern would be the way the sphere of influence has been quantified above. It is possible to imagine orbital distributions around the assumed black hole, which are such that the influence of the central IMBH is felt at radii much lower than ($< 1/4$ times lower than) the estimated value of 0.041pc . In other words, it is possible that r_s is not necessarily the radius where the central dispersion equals the circular speed around the black hole. In this case too, the density might steepen up and the mass profile turn horizontal inner to where the edge of the first radial bin is with the currently available radial resolution. In this case, we can conclude that the upper limit on the mass of the hypothesized central IMBH will be $\sim 1000M_\odot$.

Acknowledgement

I am indebted to the following people for their helpful criticisms and suggestions that contributed towards this paper: Carlton Pryor, Michael Merrifield, Laura Ferrarese, Simon Portegies Zwart and Prasenjit Saha. Prasenjit Saha is also acknowledged as the co-author of CHASSIS. The author was supported by a Royal Society Dorothy Hodgkin Fellowship.

REFERENCES

- Bahcall, J. N., and Wolf, R. A., 1976, *ApJ*, 209, 214.
- Baumgardt, H., Makino, J. and Ebisuzaki, T., 2004, *ApJ*, 613, 1133.
- Baumgardt, H., Makino, J. and Ebisuzaki, T., 2004, *ApJ*, 613, 1143.
- Baumgardt, H., Hut, P., Makino, J., McMillan, S., and Portegies Zwart, S., 2003a, *ApJ*, 582, 21.
- Baumgardt, H., Hut, P., Makino, J., Portegies Zwart, S., and McMillan, S., 2003b, *ApJ*, 589, L25.
- Baumgardt, H., Heggie, D., Hut, P., Makino, J., 2003c, *MNRAS*, 341, 247.

- Chakrabarty, Dalia, and Portegies Zwart, S., 2004, *AJ*, 128, 1046.
- Chakrabarty, Dalia, and Saha, P., 2001, *AJ*, 122, 232.
- Cropper, M., Soria, R., Mushotzky, R. F., Wu, K., Markwardt, C. B., and Pakull, M., 2004, *MNRAS*, 349, 39.
- Dull, J. D., Cohn, H. N., Murphy, B. W., Seitzer, P. O., Callanan, P. J., Rutten, R. G. M., and Charles, P. A., 2003, *ApJ*, 585, 598.
- Dull, J. D., Cohn, H. N., Murphy, B. W., Seitzer, P. O., Callanan, P. J., Rutten, R. G. M., and Charles, P. A., 1997, *ApJ*, 481, 267.
- Gebhardt, K., Pryor, C., Williams, T. B., Hesser, J. E., and Stetson, P. B., 1997, *AJ*, 113, 1026.
- Gebhardt, K., Pryor, C., O’Connell, R. D., Williams, T. B. and Hesser, J. E., 2000, *AJ*, 119, 1268.
- Gerssen, J., van der Marel, R. P., Gebhardt, K., Guhathakurta, P., Peterson, R. C., and Pryor, C., 2003, *AJ*, 125, 376.
- Gerssen, J., van der Marel, R. P., Gebhardt, K., Guhathakurta, P., Peterson, R. C., and Pryor, C., 2002, *AJ*, 124, 3270.
- Harris, W. E., 1996, *AJ*, 112, 1487.
- McNamara, B. J., Harrison, T. E., and Baumgardt, H., 2004, *ApJ*, 602, 264.
- McNamara, B. J., Harrison, T. E., and Anderson, J., 2003, *ApJ*, 595, 187.
- Meylan, G., and Heggie, D.C., 1997, *ARA&A*, 8, 1.
- Miller, M. C., and Colbert, E. J. M., 2004, *IJMPD*, 13, 1-64.
- Miller, M. C., and Hamilton, D. P., 2002, *MNRAS*, 330, 232.
- Portegies Zwart, S.F., Baumgardt, H., Hut, P., Makino, J., and McMillan, S.L.W., 2004, *Nature*, 428, 724.
- Portegies Zwart, S., and McMillan, S. L. W., 2002, *ApJ*, 576, 899.
- Portegies Zwart, S.F., Makino, J., McMillan, S.L.W., and Hut, P., 2002, *ApJ*, 565, 265.
- Portegies Zwart, S.F., McMillan, S.L.W., Hut, P., and Makino, J., 2001, *MNRAS*, 321, 199.

Roberts, T. P., Warwick, R. S., Ward, M. J., and Goad, M. R., 2004, MNRAS, 349, 1193.

Spitzer L. J., 1987, *Dynamical Evolution of Galaxy Clusters*, Princeton University Press, New Jersey.

Sosin, C., and King, I. R., 1997, AJ, 113, 1328.

Terashima, Y., and Wilson, A. S., 2004, ApJ, 601, 735.

Trager, S. C., King, I. R., and Djorgovski, S., 1995, AJ, 109, 218.

Table 1: Description of the eight different runs that are carried out with the radial velocity data. These runs are characterized by distinct choices of the initial configurations for the density and distribution function. These guesses are of the forms represented in Equations 3 and 4 which involve the parameters α , β & r_c and γ respectively. Two runs are carried out with two widely different values of any one of these four parameters; while this parameter is being changed, the other three are maintained constant. Any dependence of the results on the choice of the initial seed would imply that the algorithm is not functioning properly.

Name	α	β	$r_c(\text{pc})$	γ
RUN1	3.8	2	0.001	1
RUN2	3.8	3	0.001	1
RUN3	1.8	1	0.001	1
RUN4	5.8	1	0.001	1
RUN5	3.8	1	0.1	1
RUN6	3.8	1	0.00001	1
RUN7	3.8	1	0.001	5
RUN8	3.8	1	0.001	0.001

Table 2: Summary of results from the different runs described in Table 1. All the recovered density profiles are noted to be cored; the core size forms the second column of the following table. The mass that is calculated to lie enclosed within the innermost radial bin is cited as the next column. The projected velocity dispersion profiles estimated from the distribution function and density distributions that are recovered from the runs are all found to be consistent with the observed profile presented in Gerssen et al. (2002). Profiles of mass-to-light ratio calculated from the projection of the recovered density profiles are also noted to be consistent with the profiles presented in Dull et al. (2003)

Name	Size of core of density profile (pc)	Mass within 0.0105pc (M_{\odot})
RUN1	0.0525	1053_{322}^{328}
RUN2	0.0420	1175_{545}^{734}
RUN3	0.0420	1427_{661}^{298}
RUN4	0.0525	1005_{304}^{219}
RUN5	0.0525	948_{334}^{412}
RUN6	0.0525	1005_{305}^{176}
RUN7	0.0525	771_{192}^{360}
RUN8	0.0315	952_{326}^{300}

Fig. 1.— Figure displaying the observed data used as input for the inverse algorithm. The radial velocity measurements of 64 stars in the central core of M15 (Gerssen et al. 2003) are plotted as open circles, against projected radii. What is plotted in the figure is the absolute of the difference between a measured radial velocity and the mean of the distribution of the measured radial velocities (-103.35kms^{-1}). The proper motions of 1764 stars in M15 as measured by (McNamara, Harrison & Anderson 2003) are transformed into transverse velocities and are plotted as crosses against projected radii (after scaling the transverse velocities by $\sqrt{2}$ to account for the fact that two components of the velocity vector go into defining a transverse velocity value).

Fig. 2.— The three dimensional (luminous and dark) mass density (upper panels) and the distribution of the mass-to-light ratio (lower panels) of M15 as recovered by CHASSIS when radial velocities of Gerssen et al. (2002) are implemented as inputs to runs RUN1 & RUN2 (left), RUN3 & RUN4 (middle) and RUN5 & RUN6 (right). These runs are characterized by different choices of the guess for the cluster density, as parameterized by values of three different parameters listed in Table 1. The functional forms of the guesses for the density and distribution function are given in Equations 3 and 4. The open circles superimposed by the error bars in solid lines represent the results obtained from RUN1, RUN3 and RUN5 while the crosses with the error bars in broken lines mark the results from RUN2, RUN4 and RUN6. In the upper panels, the guess for the cluster density profile that the algorithm starts with is also shown. In RUN1, RUN3 and RUN5, the initial configuration is represented by the curve in solid line while the same in RUN2, RUN4 and RUN6 are shown in broken lines. The guess for the density, as represented here, has been normalized to the value of the central density that is recovered from the corresponding run. Density profiles recovered from the different runs are consistent with each other within the error bars and consistently display a core which is about 0.0525pc long in most cases. The calculation of the mass-to-light ratio follows from the discussion in Section 4.

Fig. 3.— Enclosed mass (top) and line-of-sight velocity dispersion (bottom) profiles of M15 as estimated from the distribution function and density that were recovered from runs RUN1 & RUN2 (left), RUN3 & RUN4 (middle) and RUN5 & RUN6 (right). As in Figure 2, open circles and errors in solid lines represent the results from RUN1, RUN3 and RUN5 while crosses superimposed with error bars in broken lines correspond to the profiles recovered from RUN2, RUN4 and RUN6. The results from the run done with the proper motion data is shown in crosses; these profiles are marked with much smaller error bars than those from the STIS data runs, owing to the much higher number of velocity measurements in the transverse velocity data set (~ 30 times more). To aid the visual comparison of the profiles, results from the radial velocity run are displayed at only few intermediate radii in the range where the radial velocity and proper motion runs overlap.

Fig. 4.— Total mass density (left) and mass-to-light ratio of M15 obtained from RUN7 and RUN8. These are runs that are characterized by a fixed choice of the initial guess for the density distribution but varying forms of the initial distribution function that the algorithm iterates upon. These forms are parametrized by the parameter γ that is described in Equation 4 and values of which for these two runs are listed in Table 1. The density distribution recovered from RUN7 is shown by open circles and solid lines while the same for RUN8 is shown in crosses and broken lines. Again, as in the other runs, these density profiles display a core in the centre and the mass-to-light profiles are noted to rise quickly at the centre.

Fig. 5.— The enclosed mass profile (left) and projected velocity dispersion profile (right) as derived from the density and distribution functions that were recovered from RUN7 (open circles and solid lines) and RUN8 (crosses and broken lines). The profiles obtained from the proper motion run are superimposed in crosses on these distributions. As in Figure 3, results have been displayed at intervals, to avoid crowding. The mass and dispersion profiles shown above are found to be consistent with those displayed in Figure 3.

Fig. 6.— Figure showing the risks of assuming an elliptic system to be spherical (left) and a system marked by velocity anisotropy, to be isotropic (right). In the former case, the integral of the density ρ over all radii r is overestimated by the simplistic assumption of sphericity, i.e. the enclosed mass is overestimated at all radii larger than the semi-minor axis of the ellipse. Similarly, the mistaken assumption of isotropy in velocity space leads to an overestimation of the integral of the distribution function f over all velocities v , i.e. the number density is overestimated. This can be a reason why the algorithm predicts larger densities than is true, at the upper end of the radial scale used in the radial velocity runs (around 1pc), thereby recovering a cluster mass in excess of what has been predicted before.